Comparing Tandem Cell Designs for Electrochemical CO_2 Reduction to Ethylene

Tobias A. Kistler[1,2], Mohammed H. Abouremeleh[1], Ryan A. Rivera[1], Erik E. Jackson[1], Yesol Kim[1,2], Finn Babbe[1,2], Peter Agbo[1,2,3,*]

[1]Chemical Sciences Division, Lawrence Berkeley National Laboratory, Berkeley, California 94720, USA

[2]Liquid Sunlight Alliance, Lawrence Berkeley National Laboratory, Berkeley, California 94720, USA

[3]Molecular Biophysics & Integrated Bio-imaging Division, Lawrence Berkeley National Laboratory, Berkeley, California 94720, USA

[*]Corresponding Author: pagbo@lbl.gov

Abstract

Electrochemical carbon dioxide reduction (CO_2R) is a promising approach for decentralized production of fuels such as ethylene (C_2H_4). However, use of Cu, the most efficient metal CO_2R catalyst for generation of C_2H_4 known to date, generally yields a product stream with poor selectivity. In an effort to increase selectivity, the reaction from CO_2 to C_2H_4 can be broken down into two steps using tandem CO_2R electrolyzers: formation of CO from CO_2, and subsequent reduction of CO to C_2H_4. Here, we present two novel tandem electrolyzer architectures that closely integrate two cathodes, one for CO generation and one for conversion to C_2H_4, while still enabling independent electrical control of the cathodic surfaces. Cathode segmentation in each of these designs also permits the controlled sequencing of mass flow of chemical intermediates in the order of Au to Cu cathode catalysts, in contrast to earlier work relying on uncontrolled, passive diffusion to facilitate the flow of chemical intermediates between catalysts. When comparing the performance of the newly-developed electrolyzer cell designs with a dual electrolyzer system, we found that the dual electrolyzer system yields the highest C_2H_4 faradaic efficiencies (FEs) of 31% and C_2H_4 concentrations (~8 mol%). However, a single Cu-containing electrolyzer outperformed all three tandem systems in terms of C_2H_4 FE (34%). Our findings, enabled by independent control of the two tandem cathode surfaces, indicate that tandem CO_2R systems need to be evaluated carefully by testing at various relevant current densities.

Keywords

Cascade, Carbon Dioxide, Electrolysis, C_2H_4, Fuel Production, Dual Cathode, Electrolyzer

Introduction

A growing global population and increasing living standards demand more and more fuels;[1] currently, these are produced mostly from fossil sources at centralized locations, posing availability concerns and potentially requiring energy-intensive distribution to end users. A promising alternative may involve the local production of fuels from widely available reactants such as carbon dioxide (CO_2) in the atmosphere.[2] CO_2 can be reduced electrochemically to a wide range of products,[3] including carbon monoxide (CO) and ethylene (C_2H_4), a precursor for gasoline through oligomerization. While CO_2 reduction (CO_2R) to CO has been achieved at faradaic efficiencies (FEs) higher than 90%,[4] yielding CO concentrations exceeding 70% in device effluent,[5] the reduction to C_2H_4 still lags behind in terms of efficiency. The only known metal catalyst to enable reduction of CO_2 to C_2H_4 in appreciable amounts is Cu, which generally yields byproducts such as CO, ethanol and hydrogen (H_2).[6,7] In an effort to increase the selectivity of Cu towards C_2H_4, researchers have tuned the microenvironment and structure of the Cu catalyst, with notable results showing C_2H_4 FEs exceeding 70%,[8,9] while C_2H_4 product concentrations have mostly been under 10%.[5]

An alternative approach is tandem CO_2R, where the reduction of CO_2 to C_2H_4 is split into two spatially separated steps on two catalysts made of different materials.[10,11] The first step typically involves CO_2R to a CO intermediate,[12] with a second step of CO reduction to C_2H_4. These two steps can be coupled on the atomic scale between two neighboring active sites or on the macroscopic scale, where two catalysts are deposited on separate portions of the electrolyzer cathode or placed in separate electrolyzer cells.[13,14] A major challenge with tandem CO_2R lies in moving the intermediate product of the first step (CO) to the active sites of the second catalyst. While a large fraction of reported tandem CO_2R electrolyzers rely on free diffusion of the intermediate to the second catalyst,[15–26] systems with more control over fluxes of reaction

intermediates are highly desirable to minimize the concentration of unreacted intermediate in the system effluent.[27–33]

Inspired by the more efficient generation of C_2H_4 from CO compared to CO_2, we developed two unique, membrane-electrode-assembly-type device architectures, that guide the flow of CO intermediate directly onto the second catalyst, aiming for maximum conversion of CO to C_2H_4. The first device employs an electron-conductive membrane made in-house, enabling the use of a cathode stack with two individual catalysts that can be operated at different potentials. After optimization of the individual components, we successfully generated C_2H_4 with this device, but the efficiency was comparatively low, mainly due to increased resistive losses. With our second developed device, which employs an anode sandwiched between two distinct cathodes, we were able to increase the C_2H_4 FE from 2 to 26%. Compared to the more integrated devices, a system containing two separate electrolyzers (with two anodes total and identical cathodes) yielded an C_2H_4 FE of 31%. These results alone signal the critical influence that system geometry and architecture will necessarily play in the future development and optimization of tandem cascade devices, even for a common materials set.

By depositing the two cathode catalysts onto separate electrodes, we were able to turn the CO-generating cathode on and off. With the CO-generating cathode off, we found that the Cu cathode can yield equal or higher FEs for C_2H_4, similar to a previous publication which reported that Cu alone can generate enough CO intermediate.[34] Our findings indicate that thorough investigations at all relevant current densities for each contributing electrode are required to fully understand the behavior and any possible advantages of a given tandem CO_2R structure.

Experimental Section

Preparation of electrodes and electrolytes

For the anode, a platinized Ti mesh with a thickness of ~270 μm was used as the substrate and coated with 100 nm of Ir by radio frequency sputtering. Anodes were reused up to 5 times, and sonicated in water in between uses. A fresh 100 nm layer of Ir catalyst was sputtered before reusing the anode. For the cathode, various substrates were used, including carbon paper with hydrophobic, microporous layer (MPL) from AvCarb Material Solutions (GDS2230 with a thickness of ~275 μm), carbon paper without MPL from CeTech (CT GDS090S with a thickness of ~90 μm), Toray carbon paper without MPL (TGP-H-60 from Alfa Aesar with a thickness of ~200 μm), and hydrophobic PTFE membranes from Sterlitech Corporation (QL211, polypropylene backing layer, ~215 μm thick) and from Hangzhou Cobetter Filtration Equipment (PTFE-003HS, ~35 μm thick). We note that the PTFE-003HS substrates were always supported by an AvCarb carbon paper between the PTFE membrane and cell endplate during electrolysis testing and that PTFE membrane refers to the PTFE-003HS membrane in this manuscript unless otherwise mentioned. Gold and copper catalysts were sputtered onto the cathode substrates with thicknesses varying from 100-500 nm. After sputtering, the anodes and cathodes were laser-cut to the right size (2 x 2 cm^2 if not mentioned otherwise). The settings of the 50 W fiber laser for the anode were 70-100% power, 1000 in s^{-1}, 20 kHz and for the cathode 10-30% power, 1000 in s^{-1}, 20 kHz. Electrodes containing PTFE substrates were carefully cut by hand with scissors using a 3D-printed mask.

Some cathodes were additionally treated with a spray coating step. After sputtering 300 nm Au on a 25 cm^2 piece of CeTech carbon paper, 0.51 g of a 5 wt% PiperION anion exchange dispersion was mixed with 12 mL isopropyl alcohol and 10 mL Milli-Q water (resistivity > 18.2 MΩ cm), followed by sonication of the ink for 1 h. Spray coating was performed using a SONOTEK ExactaCoat with a bed temperature of 80 °C and a deposition rate of 0.2 ml min^{-1}, totaling 5 mL of ink on each side.

Potassium bicarbonate ($KHCO_3$) electrolytes were prepared using ACS reagent-grade powder from Sigma-Aldrich and Milli-Q water, while potassium hydroxide (KOH) electrolytes were prepared using ACS reagent grade pellets from Sigma-Aldrich and Milli-Q water.

Preparation of cells and components

All electrolyzer cells were held together by 0.25 in thick cast poly(methyl methacrylate) (PMMA, from McMaster-Carr) endplates, which were machined in-house using a Bantam Tools Desktop CNC Milling Machine. The CAD files are available upon request. Unless otherwise mentioned, Selemion AMV membranes in chloride form from AGC Engineering with a thickness of ~100 μm were used as separators between anode and cathode. For some tests, mechanically reinforced, 15 μm thick PiperION membranes in bicarbonate form (Fuel Cell Store) were used as well. The Selemion membranes were stored in Milli-Q water and assembled wet, while the PiperION membranes were assembled dry without pretreatment. High-temperature silicone rubber sheets with a thickness of 0.01-0.02 in (10A or 20A Durometer) from McMaster-Carr were used as gaskets. A 50 W fiber laser was used to cut the silicone gaskets (5-15% power, 39.37 in s^{-1}, 50 kHz). Tantalum foils with a thickness of 0.001 in were used to establish electrical contact between the electrodes and potentiostats. Before cell assembly, the endplates, gaskets and Ta foils were sonicated for 1 h in 10% nitric acid (made from 70% ACS reagent grade nitric acid from Sigma-Aldrich), followed by a Milli-Q water bath to rinse off the nitric acid and sonication for 1 h in fresh Milli-Q water, keeping anodic and cathodic components in separate beakers to avoid cross-contamination. Following sonication, the components were blown dry with N_2. After stacking of all cell components including membrane(s) and electrodes, using separate tweezers for anodic and cathodic parts, the cell was tightened using stainless steel screws and a torque screwdriver keeping cell compression consistent across tests.

Measurement conditions

Unless otherwise mentioned, the following conditions were used during electrolysis testing. Anolyte (1M $KHCO_3$) was circulated at 6 ml min^{-1} through the anode using a peristaltic pump. Mass flow controllers (Alicat Scientific) were used to control the dry cathodic gas flow rate of CO or CO_2 in a range of 0.5-5 sccm. Potentiostats from Biologic were used to control the cell voltage or current in a 2-electrode configuration. Generally, the electrolyzer anode was used as the working electrode and the cathode as the counter/reference electrode, yielding positive voltage/current signals. However, for electrolyzers containing two cathode layers, the single anode was used as the common counter/reference electrode, while each cathode was connected to the working electrode cables of individual potentiostat channels. The latter configuration yielded negative voltage/current signals, but the absolute values were used for plotting and efficiency calculations. Additionally, the cumulative current of the whole system was considered for relevant efficiency calculations. Linear sweep voltammetry or cyclic voltammetry scans were typically carried out before and after the constant voltage/current measurements.

Gas product analysis

Cathodic gas product concentrations were quantified using an SRI Instruments (Multiple Gas Analyzer #5, 8610C, 0.1 ml sample loop volume) gas chromatograph (GC) with thermal conductivity and flame ionization detectors, and a methanizer for quantification of CO and CO Anodic gas product concentrations were quantified using an Agilent 7890A GC equipped with a thermal conductivity detector. The gas flow rates at the outlets of the electrolyzers were carefully monitored using mass flow meters (Alicat Scientific) and used for faradaic efficiency calculations.

Liquid product analysis

Liquid products generated in the cathode and collected in the anolyte were quantified with a Nuclear Magnetic Resonance (NMR, 500 MHz Bruker) instrument. The internal standards for quantification were 0.05M phenol and 0.01M dimethyl sulfoxide. The water peak was suppressed with a pre-saturation sequence. NMR samples were prepared with 400 μL of anolyte, 50 μL of internal standard solution and 50 μL of D_2O. A more detailed description of the quantification process used here is described by Prabhakar et al. and Chatterjee et al.[35,36]

Scanning Electrode Microscope (SEM)

An FEI Quanta 250 FEG SEM system was used to analyze surface morphologies.

X-ray photoelectron spectroscopy (XPS)

A Kratos Axis Ultra DLD system was used to analyze the chemical composition of Cu- and Au-based electrodes at a take-off angle of 0° relative to the surface normal. An Al Kα source was used for excitation (hν = 1486.6 eV). The pass energy was set to 20 eV and a step size of 0.1 eV was used for the core levels (Cu 2p and Au 4f) and the Cu Auger line. A pass energy of 160 eV and a step size of 1 eV were used for the survey scans.

Results and Discussion

Testing a single Cu electrode with CO_2 and CO feeds

Tandem CO_2R electrolysis systems are motivated by the assumption that highly reduced products, such as ethylene, can be produced more efficiently and selectively from CO compared to CO_2. To examine whether this assumption holds true with the materials we used, we tested a

CO_2 electrolyzer containing a Cu-sputtered cathode and switched between CO_2 and CO cathode feeds (Fig. 1).

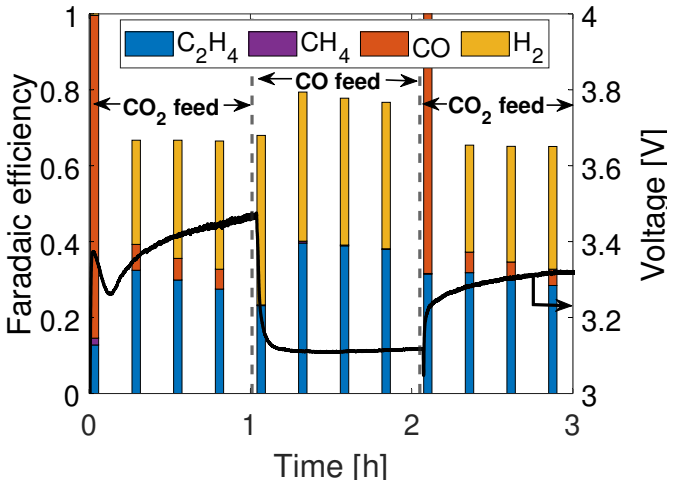

Fig. 1 Faradaic efficiency (bar data) and voltage (line data) as a function of time switching between CO_2 and CO cathode feeds. This electrolyzer was tested at a constant current of 80 mA (20 mA cm^{-2}) with a cathode inlet flow rate of 5 sccm and a cathode consisting of 300 nm sputtered Cu on thin (~35 μm) PTFE membrane substrate, supported by an uncoated AvCarb carbon paper. The high CO FE values at the beginning of the CO_2 feed phases are due to CO feed being used prior to these phases.

While C_2H_4 FE values near 30% were achieved with CO_2 feeds, the C_2H_4 FE increased to ~40% with a CO feed, indicating that significantly more C_2H_4 is produced under CO feed conditions (the difference in C_2H_4 production rate is even higher, ~100% increase, than the FE difference since C_2H_4 generation from CO requires fewer electrons than from CO_2). The FE for H_2 also increased modestly from ~31% to ~39%, and was generally more stable under CO feed conditions. Under CO feed conditions, fewer products containing one carbon atom (C) are expected since rearrangements to CO and formate are unlikely, increasing the chances of C-C bonding to C_{2+} products such as C_2H_4. Furthermore, the total FE of gas products is also higher

under CO feed conditions, indicating that fewer liquid products are formed compared to CO_2 feed conditions.

In principle, it is possible to quantify the formation of liquid products with tools such as NMR or High Performance Liquid Chromatography. However, electrolyzers containing no catholyte make this difficult, since most liquid products are expected to cross the membrane separating the anode and cathode. After crossing the membrane, these liquid products can get re-oxidized, complicating the calculation of accurate liquid FE values.[37] In Fig. S1, the FE is shown for gas products collected at the cathode outlet and liquid products collected in the anolyte for an experiment run at the same conditions as the CO_2 feed steps in Fig. 1, indicating that a large fraction of FE is unaccounted for due to liquid product crossover and re-oxidation. Alternatively, the FE of oxygen exiting the anode compartment can be determined using a GC, similar to the calculation of cathodic gas FEs, to estimate the amount of liquid product re-oxidation. Since O_2 is the only expected oxidation product in the anode, any FE value lower than 1 for O_2 would indicate that cathodic products re-oxidize at the anode. As shown in Fig. S2, the FE of O_2 is significantly lower than 1 using a Cu catalyst and follows the trend of cumulative, cathodic gas FEs, indicating that most cathodic liquid products do indeed cross the membrane and re-oxidize at the anode.

Consistent with previous literature,[6,38–40] the voltage during the CO feed phase is significantly lower than during the CO_2 phases, because CO_2 is a very stable molecule that requires more energy to be activated. Furthermore, the CO coverage of catalyst sites is expected to be higher with a CO feed, facilitating C-C coupling compared to a CO_2 feed. Finally, the slightly increased rate of H_2 evolution, which generally requires lower overpotentials, also contributes to the lower cell voltage observed during the CO feed phase.

Optimization of Tandem Components

After establishing the benefits of CO reduction over CO_2R, we continued with the development of a tandem CO_2R device that reduces CO_2 to CO on a first cathode, followed by further reduction of CO intermediates to C_2H_4 on a second cathode. Our developed device architecture enforces the directional flow of the intermediate onto the second catalyst in the tandem structure, compared to other systems relying on free diffusion of the intermediate (Fig. 2).

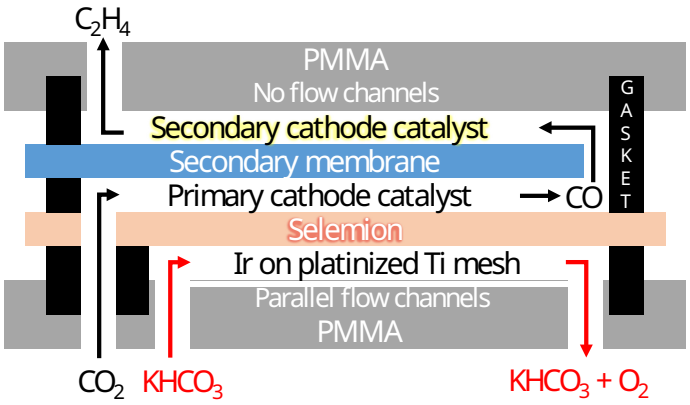

Fig. 2 General schematic of the 3-layer Cathode Tandem CO_2R electrolyzer. The dimensions are not to scale but have instead been adjusted to aid visualization of all layers. CO_2 is fed to the primary cathode catalyst layer which generates CO. The CO is then forced through the secondary cathode catalyst layer to generate C_2H_4. The two cathodes are separated by an ion exchange membrane (which can be fabricated to be electrically conductive) to prevent direct gas flow between the layers but enable ion (and electron) transport. An anion exchange membrane (Selemion), with a small hole to enable CO_2 flow onto the primary cathode from the anode side, separates the 3-layer cathode from the anode (Ir on Ti). Anolyte ($KHCO_3$) is circulated through the anode compartment. Poly(methyl methacrylate) (PMMA) endplates and silicone gaskets (shown in black) seal the electrolyzer from the environment. We note that the primary cathode can also generate byproducts such as H_2 and the secondary cathode can form byproducts such as H_2, CO, CH_4 and ethanol, depending on the chosen catalyst and

measurement conditions.

Initially, we developed this device with a conductive, cation-exchange secondary membrane[38,39] ('Condubrame'), requiring just a single electrical contact between the 3-layer cathode stack and a potentiostat (Fig. S3). While we were able to show that the secondary cathode catalyst was active in a simplified device and yielded CO_2R products, the overall efficiency was quite low, partially due to the bipolar interface between the Nafion-containing Condubrame and Selemion. The Nafion content of the Condubrame also results in an ionomer with acidic character, which likely drives excessive hydrogen evolution in the device. We also attempted fabrication of an electron-conductive anion-exchange membrane (AEM), but we were unable achieve stable blended emulsions between known anionic ionomers and the conductive polymer PEDOT:PSS. However, successful fabrication of a conductive AEM would likely increase the efficiency of such a cathode stack. Any further testing of the 3-layer Cathode Device was done with a commercially available PiperION secondary membrane, which is an electrically insulating material. While two potentiostats, contacting each cathode substrate individually, were required to test the PiperION-containing devices, this structure also enabled us to separately control the applied voltage of each cathode.

Afterwards, we moved on to optimize the two cathodes shown in Fig. 2. It is important to note that the primary cathode layer (the cathode proximate to the anode) must also be ion-conducting through its cross-section, restricting the options on how this layer can be fabricated. Therefore, it was crucial to decide if the CO-generating or the CO-converting catalyst should be placed closer to the anode (and adjust the CO_2 flow direction accordingly). We started with testing a Cu-containing cathode for conversion of CO to C_2H_4, made by spray coating an ink that contained Cu nanoparticles and Sustainion anion exchange ionomer. This electrode generated some C_2H_4 but regardless of the substrate used, H_2 was the dominant product (Fig. S4), likely

247 the cause of electrode flooding observed during operation. Meanwhile, an ionomer-
248 impregnated, Au-containing primary cathode for generation of CO performed much better than
249 the comparable Cu cathode, yielding CO FEs exceeding 90% and CO concentrations higher
250 than 40% (Fig. S5). Since the CO-generating cathode yielded much more target product than the
251 CO-converting cathode under the constraints necessary for the cathode layer closer to the anode,
252 we picked Au as the primary cathode catalyst.

253 After picking the primary cathode catalyst, we continued with optimizing the secondary
254 cathode catalyst. Since this layer does not need to be fully ion-conductive, its hydrophobicity
255 can be tuned to a greater extent. Due to the poor performance of the Cu catalyst in a hydrophilic
256 environment (Fig. S4), we decided to increase the hydrophobicity of this layer significantly.
257 While spray-coating PTFE particles on top of a Cu-sputtered AvCarb carbon paper reduced the
258 C_2H_4 FE noticeably (Fig. S6), sputtering Cu directly on top of a PTFE substrate increased the
259 C_2H_4 FE from 11 to 29% when compared to the carbon paper substrate (Fig. S7). Furthermore,
260 we compared different thicknesses of PTFE substrate, and noticed a decline in C_2H_4 FE when
261 the total cathode thickness was reduced (Fig. S8). We attribute this decline in FE to less ideal
262 compression at the reduced cathode thickness, which has been shown to lower the FE of CO_2R
263 products while increasing the H_2 FE.[40] Additionally, we compared constant potential to pulsed
264 potential operation, which in some cases has been found to increase the durability and
265 selectivity for C_2H_4.[41] However, under the timescales and conditions tested, we found no
266 significant change to the C_2H_4 FE (Fig. S9). Coating a Cu cathode with a previously reported
267 additive that impedes proton transport[42] increased the FE for C_2H_4 with a CO_2 feed, but we were
268 unable to produce the same effect with a CO feed, likely because this additive film is also
269 limiting the diffusion of CO (Fig. S10).[43]

270 We tested our optimized configuration of the secondary cathode catalyst (sputtered Cu
271 on thin PTFE membrane) for an extended period under CO feed conditions. The peak C_2H_4 FE

of 41% dropped to about 33% after 4 h, indicating that changes to the C_2H_4 FE are limited during this timeframe (Fig. S11a). Since this test was run at flow rates that yielded the highest CO concentrations with the primary cathode (~0.5 sccm, Fig. S5), we diluted the cathode outlet with an inert gas before flowing into the GC sample loop (Fig. S11b), ensuring the precise determination of C_2H_4 FE values even at high C_2H_4 cathode outlet concentrations. Such low inlet flow rates would be problematic with a pure CO_2 feed while keeping the remaining conditions the same, because CO_2 can react with hydroxide ions to form carbonate and bicarbonate ions, that can subsequently cross the membrane to the anode.[44] With that additional reaction pathway for CO_2, C species starvation will become an issue in our system at flow rates ~0.5 sccm, as demonstrated by significantly increased amounts of H_2 when moving from 1 sccm to 0.5 sccm (Fig. S12). Interestingly, the C_2H_4 FE was higher at 1 sccm than at 5 sccm CO_2 flow rate, likely due to the increased residence time of gases in the cell, which aids the conversion of intermediate species such as CO.

Finally, we also tested configurations utilizing a thinner primary membrane (PiperION 15 instead of Selemion), which reduced the voltage needed to operate at the same current. However, our cathodes flooded quickly when using this separator, leading to vastly increased H_2 FEs, and rendering PiperION 15 unsuitable as our primary membrane. Similarly, using a Ni anode catalyst lead to quick delamination under the near-neutral pH conditions imposed by the anolyte (1M $KHCO_3$) and was not investigated further. Finally, different cathode flow field geometries (single serpentine vs. parallel vs. no channels) yielded no significant changes in electrolyzer performance.

After deciding on the final composition of the 3-layer Cathode Tandem CO_2R electrolyzer, as shown in Fig. 2, we investigated the surfaces of the primary and secondary cathodes with XPS. XPS data of the primary cathode indicate the presence of metallic Au and PiperION ionomer on the surface (Fig. S13). While the exact distribution of Cu oxidation states

297 on the secondary cathode is not clear from our XPS data, partial oxidation of the sputtered,
298 metallic Cu layer became obvious (Fig. S13).
299
300 **Testing of Different Tandem Architectures**
301 After optimizing the individual layers of the 3-layer Cathode electrolyzer shown in
302 Fig. 2, we assembled a complete device (Fig. 3a), and compared it to another tandem
303 architecture (Anode Center device, Fig. 3b) and a Dual Electrolyzer CO_2R system (Fig. 3c).

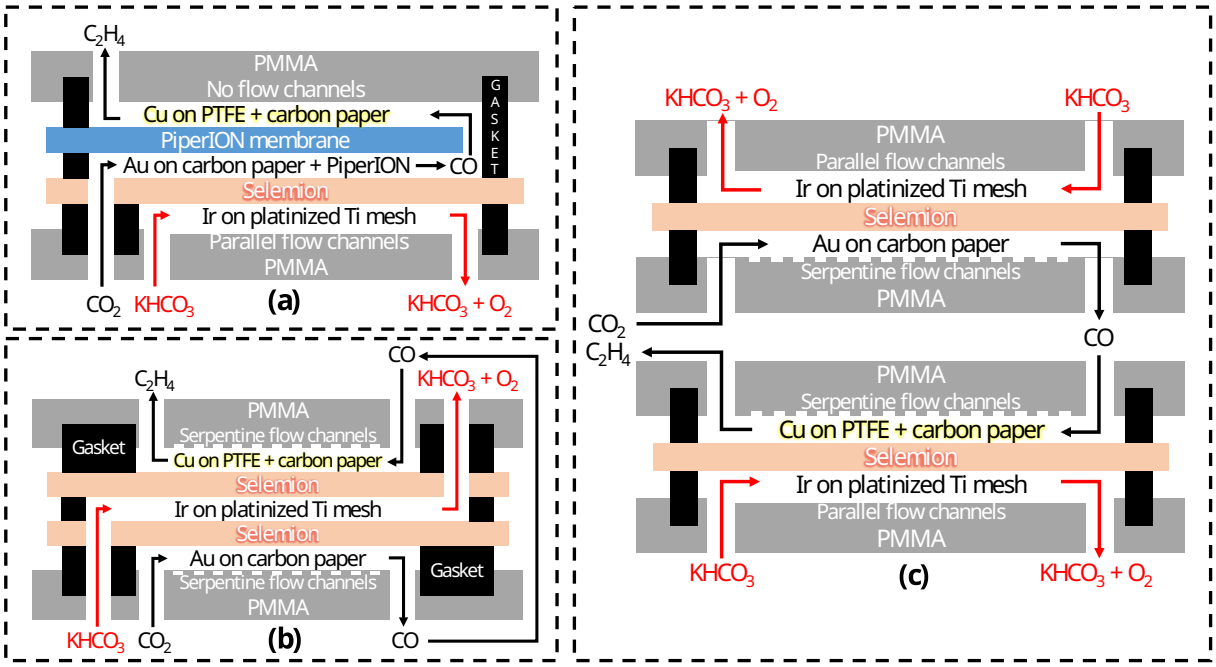

Fig. 3 Schematics of three different electrolyzer device systems, each utilizing two cathode catalysts for tandem CO_2R. The dimensions are not to scale but have instead been adjusted to aid visualization of all layers. (a) 3-layer Cathode device from Fig. 2 with Au as the primary cathode catalyst (100 nm each on both sides, 1.97 x 2.67 cm^2) and Cu as the secondary catalyst (300 nm on the anode-facing side, 1.91 x 2.37 cm^2), separated by a 15 μm thick PiperION anion exchange membrane. Since this membrane is electrically insulating, both cathodes need to be connected separately to a potentiostat. The cathode contains no flow channels, forcing all gas flow through the pores of the carbon paper and PTFE sheet, while the anode endplate provides parallel flow

channels to guide anolyte from inlet to outlet. (b) Anode Center device placing the anode (with Ir coating on both sides, 2 x 2.95 cm^2) in the middle, sandwiched by two Selemion membranes and the respective cathodes (coated with 100 nm of Au and 300 nm of Cu, 2 x 2 cm^2). The intermediate product CO flows externally from the primary to the secondary cathode and the Selemion membranes contain small holes to enable continuous anolyte and oxygen product flow. The cathodes contain serpentine flow channels, enabling all gas components to flow through the flow channels or through the carbon paper, while the anode contains no flow channels forcing all anolyte through the pores of the Ti mesh. (c) Dual Electrolyzer CO_2R system, containing two separate electrolyzers, one with a 100 nm Au cathode catalyst and one with a 300 nm Cu cathode catalyst. The cathodes contain serpentine flow channels, enabling all gas components to flow through the flow channels or through the carbon paper, while the anode endplates provide parallel flow channels to guide anolyte from inlet to outlet. It should be noted that this system requires two precious-metal anodes (Ir on Ti), and significantly more space, support structure and material than the more integrated devices shown in (a) and (b).

Although the 3-layer Cathode electrolyzer is the only device that enables internal flow of CO intermediate to the secondary cathode, the Anode Center device still offers close integration of all components and requires only a single anode substrate. In comparison to the aforementioned devices, the Dual Electrolyzer CO_2R system consists of two separate electrolyzers, which requires more anode substrate and support material. Since the primary cathodes in the Anode Center device and Dual Electrolyzer system do not need to be ion-conducting through the whole thickness of this layer, it allows for more flexibility regarding the substrate material. Therefore, a sputtered Au layer on AvCarb carbon paper was used here, which generates CO selectively as we have shown previously.[45] However, to allow for

comparison between the different architectures, the remaining components of these devices were kept as similar to the 3-layer Cathode electrolyzer as possible.

Based on the maximum achievable CO concentration with the primary cathode (Fig. S5) and therefore, maximum CO availability for the secondary cathode, we chose a CO_2 flow rate of 0.5 sccm and tested all three electrolyzer systems shown in Fig. 3. Because the primary and secondary cathode catalysts were placed on electrically-separate substrates, it was possible to individually control current flow to each catalyst. This allowed us to turn off the primary cathode completely (zero current) and analyze its impact on overall device performance (Fig. 4).

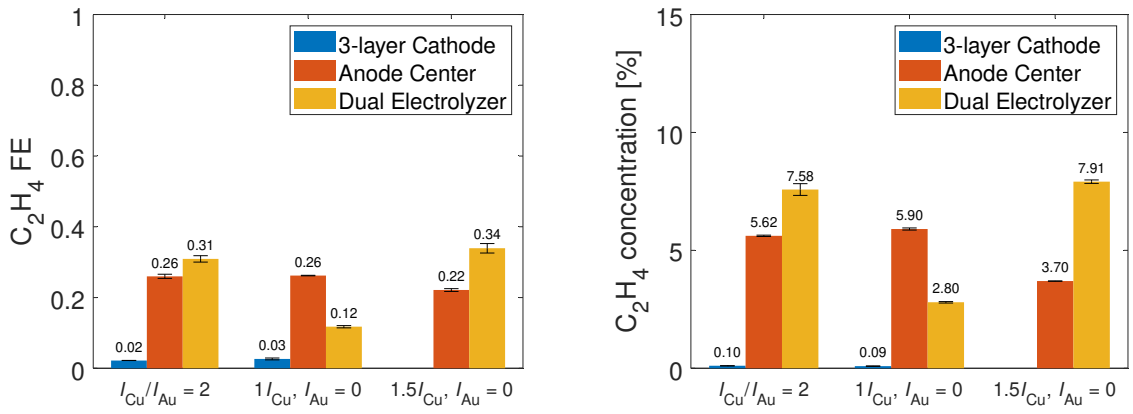

(a) (b)

Fig. 4 Quantification of ethylene formation with the devices shown in Fig. 3 at three different measurement conditions. For the first measurement condition, the current of the Cu cathode was twice the current of the Au cathode ($I_{Cu}/I_{Au}=2$); for the second condition the Cu current was kept the same, but the Au current was set to 0 ($1\,I_{Cu}$, $I_{Au}=0$), and for the third condition the Au current was kept at 0 but the Cu current was multiplied by a factor of 1.5 ($1.5\,I_{Cu}$, $I_{Au}=0$), making the Cu current at the third condition equal to the combined current of Au and Cu cathodes at the first measurement condition. All tests were conducted using a CO_2 flow rate of 0.5 sccm. (a) Mean ethylene faradaic efficiencies calculated using the last

three GC injections of every measurement condition (Fig. S14-16). The standard deviations are shown as error bars. (b) Mean ethylene concentrations (in mol%) calculated using the last three GC injections of every measurement condition (Fig. S14-16). The standard deviations are shown as error bars.

During the first measurement condition we tested, the current of the Cu cathode was set to twice the current of the Au cathode $I_{Cu}/I_{Au}=2$. We chose this condition since the number of electrons transferred to produce two molecules of CO from CO_2 is half compared to the number of electrons needed to make one molecule of C_2H_4 from two molecules of CO. At this condition, the Dual Electrolyzer system yielded the highest C_2H_4 FE (31%) and concentration (7.58 mol%) in the cathode outlet stream, followed closely by the Anode Center device. After this condition, we turned the Au electrode off for all three systems, but kept the current of the Cu electrode the same ($1\,I_{Cu}$, $I_{Au}=0$). At the second measurement condition shown in Fig. 4, operation of the Anode Center device resulted in the highest C_2H_4 FE (26%) and concentration (5.90 mol%), while the C_2H_4 FE of the Dual Electrolyzer system dropped significantly and the performance of the 3-layer Cathode device remained mostly unchanged. Finally, at the last measurement condition shown in Fig. 4, the Au current was kept at 0 but the Cu current was multiplied by a factor of 1.5 ($1.5\,I_{Cu}$, $I_{Au}=0$), making the Cu current at the third condition equal to the combined current of Au and Cu cathodes at the first measurement condition. At this condition, the Dual Electrolyzer system again yielded the highest C_2H_4 FE (34%) and concentration (7.91 mol%) in the cathode outlet stream, while the Anode Center device produced less C_2H_4 compared to the lower Cu current condition (the 3-layer Cathode device was not tested at this condition). Similar to the trends in C_2H_4 FE, the C_2H_4 energy efficiency of the Anode Center device and the Dual Electrolyzer system was also higher when the Au electrode was left unbiased (Table S1-S2).

The results of these tests show that the 3-layer Cathode device exhibits high overpotentials at comparatively low currents (Fig. S14), most likely due to high ohmic losses of the multiple cathode layers. Due to the large overpotentials, the device was not able to generate significant amounts of C_2H_4 even when using individually optimized components. Comparing the Anode Center device and Dual Electrolyzer system revealed that each of these systems have their ideal operating point for maximum C_2H_4 generation, and they seem to perform best when the Au electrode is turned off. Even at very similar operating voltages of the Cu electrodes at the $1\,I_{Cu}$, $I_{Au}=0$ (~3-3.1 V) and $1.5\,I_{Cu}$, $I_{Au}=0$ (~3.3 V) conditions (Fig. S15-16), the C_2H_4 FEs were very different between the two systems, despite employing the same catalytic materials. Such differences may be attributed to the distinct catalytic microenvironments of the respective devices that stem from their unique architectures. For example, in contrast to the Dual Electrolyzer system, O_2 bubbles cannot exit through flow channels in the Anode Center device but are instead transported through the pores of the anode substrate. The different anode conditions may alter the voltage distributions between the anodes and cathodes, effectively changing the real cathode potential, which can affect the ethylene FE.[46] Unfortunately, since there is no space for a traditional reference electrode, it is difficult to measure the cathode potential in zero-gap electrolyzers, and we were not able to confirm this hypothesis experimentally.

Independent of the tandem CO_2R approach tested, experimental conditions with the CO-generating Au cathode turned off consistently yielded the highest C_2H_4 FE and concentration values. While initially, the Dual Electrolyzer system showed decreased ethylene generation when the Au electrode was turned off ($1\,I_{Cu}$, $I_{Au}=0$ condition), increasing the Cu current while keeping the Au current at zero ($1.5\,I_{Cu}$, $I_{Au}=0$ condition) yielded the best performance for C_2H_4 generation overall. These results highlight that tandem CO_2R systems need to be

evaluated carefully to truly compare their efficiencies to single cathode devices. We note that while the C_2H_4 FE was not improved with our tandem systems, we found that the H_2/CO molar product ratio was affected significantly by the current of the Au electrode. As shown in Fig. S15-16, turning on the Au electrode generally yielded much more CO, changing the H_2/CO ratio from ~75/1 to ~3/1. These findings are consistent with previous reports that found insignificant changes to the ethylene FE by adding a CO-generating co-catalyst to Cu, but saw significant changes in the H_2/CO ratio.[47,48]

Conclusion

We showed that ethylene can be generated more efficiently from CO than CO_2R. However, the operation of three different tandem structures, each containing separate CO-generating and CO-converting cathodes, did not result in favorable C_2H_4 production compared to single Cu cathodes. Our results stand in contrast to previously published tandem systems that have shown increased C_2H_4 generation after adding a secondary co-catalyst to a Cu electrode. On the one hand, these disparate results could be explained by the different integration strategies of the co-catalysts. Many previous studies place the co-catalysts in close proximity and rely on free diffusion of CO intermediates to the Cu catalyst. The advantage of this strategy is that CO concentrations only need to be increased locally to demonstrate a beneficial effect, and high global CO_2 conversion is not required (however, maximizing CO_2 conversion would still be relevant for industrial applications). While our systems generally provide more control over CO intermediate flow, (nearly) full conversion of CO_2 without excessive H_2 evolution would be necessary to maximize the overall CO concentration and increase the efficiency of the tandem systems. However, as demonstrated by past work, reaching total CO concentrations above 50% proved to be difficult.[5] On the other hand, we also showed that our tandem CO_2R systems

outperformed comparable single cathode systems at first glance. However, varying the measurement conditions quickly revealed that the single cathode catalyst electrolyzer was able to yield the highest C_2H_4 faradaic efficiency (34%). Such findings indicate that tandem CO_2R systems need to be evaluated at multiple relevant current densities to rigorously determine the operational regimes in which they represent a net-benefit over single-catalyst electrolysis. Finally, it is worth noting that the investigated Cu catalyst was working quite efficiently for CO_2R and able to produce cathode outlet streams containing C_2H_4 concentrations of ~8%, one of the higher values found in literature.[5] Utilizing a less efficient catalyst for CO_2-to-C_2H_4 conversion that still works well for CO-to-C_2H_4 conversion is expected to increase the performance of tandem systems, because there would be less competition between CO_2R and CO reduction. Therefore, we think more research on catalysts specifically designed for CO reduction, a field that is currently underexplored, is warranted.[28,49]

Supporting Information

Additional experimental data and related methods, including XPS, SEM and NMR results (PDF).

Acknowledgements

This material is based on work performed by the Liquid Sunlight Alliance, which is supported by the U.S. Department of Energy, Office of Science, Office of Basic Energy Sciences, Fuels from Sunlight Hub under Award Number DE-SC0021266.

Copyright Statement

Conflict of Interest

The authors declare the following competing financial interest(s): The contents of this paper relate to 2023 and 2026 patent applications by Lawrence Berkeley National Laboratory, with T.K. and P.A. listed as inventors.

References

(1) Holdren, J. P. Population and the Energy Problem. *Popul. Environ.* **1991**, *12* (3), 231–255. https://doi.org/10.1007/BF01357916.

(2) Herron, J. A.; Kim, J.; Upadhye, A. A.; Huber, G. W.; Maravelias, C. T. A General Framework for the Assessment of Solar Fuel Technologies. *Energy Environ. Sci.* **2015**, *8* (1), 126–157. https://doi.org/10.1039/C4EE01958J.

(3) Nitopi, S.; Bertheussen, E.; Scott, S. B.; Liu, X.; Engstfeld, A. K.; Horch, S.; Seger, B.; Stephens, I. E. L.; Chan, K.; Hahn, C.; Nørskov, J. K.; Jaramillo, T. F.; Chorkendorff, I. Progress and Perspectives of Electrochemical CO_2 Reduction on Copper in Aqueous Electrolyte. *Chem. Rev.* **2019**, *119* (12), 7610–7672. https://doi.org/10.1021/acs.chemrev.8b00705.

(4) Jeong, H.-Y.; Balamurugan, M.; Choutipalli, V. S. K.; Jeong, E.; Subramanian, V.; Sim, U.; Nam, K. T. Achieving Highly Efficient CO_2 to CO Electroreduction Exceeding 300 mA cm^{-2} with Single-Atom Nickel Electrocatalysts. *J. Mater. Chem. A* **2019**, *7* (17), 10651–10661. https://doi.org/10.1039/C9TA02405K.

(5) Kistler, T. A.; Prabhakar, R. R.; Agbo, P. A Recirculation System for Concentrating CO_2 Electrolyzer Products. *Sustain. Energy Fuels* **2024**, *8* (10), 2292–2298. https://doi.org/10.1039/D3SE01506H.

(6) Wang, L.; Nitopi, S. A.; Bertheussen, E.; Orazov, M.; Morales-Guio, C. G.; Liu, X.; Higgins, D. C.; Chan, K.; Nørskov, J. K.; Hahn, C.; Jaramillo, T. F. Electrochemical Carbon Monoxide Reduction on Polycrystalline Copper: Effects of Potential, Pressure, and pH on Selectivity toward Multicarbon and Oxygenated Products. *ACS Catal.* **2018**, *8* (8), 7445–7454. https://doi.org/10.1021/acscatal.8b01200.

(7) Jouny, M.; Luc, W.; Jiao, F. High-Rate Electroreduction of Carbon Monoxide to Multi-Carbon Products. *Nat. Catal.* **2018**, *1* (10), 748–755. https://doi.org/10.1038/s41929-018-0133-2.
(8) Liu, W.; Zhai, P.; Li, A.; Wei, B.; Si, K.; Wei, Y.; Wang, X.; Zhu, G.; Chen, Q.; Gu, X.; Zhang, R.; Zhou, W.; Gong, Y. Electrochemical CO_2 Reduction to Ethylene by Ultrathin CuO Nanoplate Arrays. *Nat. Commun.* **2022**, *13* (1), 1877. https://doi.org/10.1038/s41467-022-29428-9.
(9) Li, J.; Wang, Z.; McCallum, C.; Xu, Y.; Li, F.; Wang, Y.; Gabardo, C. M.; Dinh, C.-T.; Zhuang, T.-T.; Wang, L.; Howe, J. Y.; Ren, Y.; Sargent, E. H.; Sinton, D. Constraining CO Coverage on Copper Promotes High-Efficiency Ethylene Electroproduction. *Nat. Catal.* **2019**, *2* (12), 1124–1131. https://doi.org/10.1038/s41929-019-0380-x.
(10) Zhang, B.; Wang, L.; Li, D.; Li, Z.; Bu, R.; Lu, Y. Tandem Strategy for Electrochemical CO_2 Reduction Reaction. *Chem Catal.* **2022**, *2* (12), 3395–3429. https://doi.org/10.1016/j.checat.2022.10.017.
(11) Sisler, J.; Khan, S.; Ip, A. H.; Schreiber, M. W.; Jaffer, S. A.; Bobicki, E. R.; Dinh, C.-T.; Sargent, E. H. Ethylene Electrosynthesis: A Comparative Techno-Economic Analysis of Alkaline vs Membrane Electrode Assembly vs CO_2 –CO–C_2H_4 Tandems. *ACS Energy Lett.* **2021**, *6* (3), 997–1002. https://doi.org/10.1021/acsenergylett.0c02633.
(12) Hori, Y.; Murata, A.; Takahashi, R.; Suzuki, S. Electroreduction of Carbon Monoxide to Methane and Ethylene at a Copper Electrode in Aqueous Solutions at Ambient Temperature and Pressure. *J. Am. Chem. Soc.* **1987**, *109* (16), 5022–5023. https://doi.org/10.1021/ja00250a044.
(13) Möller, T.; Filippi, M.; Brückner, S.; Ju, W.; Strasser, P. A CO_2 Electrolyzer Tandem Cell System for CO_2-CO Co-Feed Valorization in a Ni-N-C/Cu-Catalyzed Reaction Cascade. *Nat. Commun.* **2023**, *14* (1), 5680. https://doi.org/10.1038/s41467-023-41278-7.
(14) Sui, P.; Wang, Y.; Wang, X.; Liu, S.; Luo, J. Advances in Tandem Strategies for CO_2 Electroreduction: From Electrocatalysts to Reaction System Design. *ChemCatChem* **2025**, *17* (6), e202401604. https://doi.org/10.1002/cctc.202401604.
(15) Wang, X.; De Araújo, J. F.; Ju, W.; Bagger, A.; Schmies, H.; Kühl, S.; Rossmeisl, J.; Strasser, P. Mechanistic Reaction Pathways of Enhanced Ethylene Yields during Electroreduction of CO_2–CO Co-Feeds on Cu and Cu-Tandem Electrocatalysts. *Nat. Nanotechnol.* **2019**, *14* (11), 1063–1070. https://doi.org/10.1038/s41565-019-0551-6.
(16) Lin, Y.; Lee, D. U.; Tan, S.; Koshy, D. M.; Lin, T. Y.; Wang, L.; Corral, D.; Avilés Acosta, J. E.; Zamora Zeledon, J. A.; Beck, V. A.; Baker, S. E.; Duoss, E. B.; Hahn, C.; Jaramillo, T. F. Vapor-Fed Electrolyzers for Carbon Dioxide Reduction Using Tandem Electrocatalysts: Cuprous Oxide Coupled with Nickel-Coordinated Nitrogen-Doped Carbon. *Adv. Funct. Mater.* **2022**, *32* (28), 2113252. https://doi.org/10.1002/adfm.202113252.
(17) Liu, Y.; Qiu, H.; Li, J.; Guo, L.; Ager, J. W. Tandem Electrocatalytic CO_2 Reduction with Efficient Intermediate Conversion over Pyramid-Textured Cu–Ag Catalysts. *ACS Appl. Mater. Interfaces* **2021**, *13* (34), 40513–40521. https://doi.org/10.1021/acsami.1c08688.
(18) Gurudayal; Perone, D.; Malani, S.; Lum, Y.; Haussener, S.; Ager, J. W. Sequential Cascade Electrocatalytic Conversion of Carbon Dioxide to C–C Coupled Products. *ACS Appl. Energy Mater.* **2019**, *2* (6), 4551–4559. https://doi.org/10.1021/acsaem.9b00791.

(19) Lum, Y.; Ager, J. W. Sequential Catalysis Controls Selectivity in Electrochemical CO_2 Reduction on Cu. *Energy Environ. Sci.* **2018**, *11* (10), 2935–2944. https://doi.org/10.1039/C8EE01501E.
(20) Chen, C.; Li, Y.; Yu, S.; Louisia, S.; Jin, J.; Li, M.; Ross, M. B.; Yang, P. Cu-Ag Tandem Catalysts for High-Rate CO_2 Electrolysis toward Multicarbons. *Joule* **2020**, *4* (8), 1688–1699. https://doi.org/10.1016/j.joule.2020.07.009.
(21) Gao, J.; Zhang, H.; Guo, X.; Luo, J.; Zakeeruddin, S. M.; Ren, D.; Grätzel, M. Selective C–C Coupling in Carbon Dioxide Electroreduction via Efficient Spillover of Intermediates As Supported by Operando Raman Spectroscopy. *J. Am. Chem. Soc.* **2019**, *141* (47), 18704–18714. https://doi.org/10.1021/jacs.9b07415.
(22) Hoang, T. T. H.; Verma, S.; Ma, S.; Fister, T. T.; Timoshenko, J.; Frenkel, A. I.; Kenis, P. J. A.; Gewirth, A. A. Nanoporous Copper–Silver Alloys by Additive-Controlled Electrodeposition for the Selective Electroreduction of CO_2 to Ethylene and Ethanol. *J. Am. Chem. Soc.* **2018**, *140* (17), 5791–5797. https://doi.org/10.1021/jacs.8b01868.
(23) Wang, M.; Loiudice, A.; Okatenko, V.; Sharp, I. D.; Buonsanti, R. The Spatial Distribution of Cobalt Phthalocyanine and Copper Nanocubes Controls the Selectivity towards C_2 Products in Tandem Electrocatalytic CO_2 Reduction. *Chem. Sci.* **2023**, *14* (5), 1097–1104. https://doi.org/10.1039/D2SC06359J.
(24) Ma, Y.; Yu, J.; Sun, M.; Chen, B.; Zhou, X.; Ye, C.; Guan, Z.; Guo, W.; Wang, G.; Lu, S.; Xia, D.; Wang, Y.; He, Z.; Zheng, L.; Yun, Q.; Wang, L.; Zhou, J.; Lu, P.; Yin, J.; Zhao, Y.; Luo, Z.; Zhai, L.; Liao, L.; Zhu, Z.; Ye, R.; Chen, Y.; Lu, Y.; Xi, S.; Huang, B.; Lee, C.; Fan, Z. Confined Growth of Silver–Copper Janus Nanostructures with {100} Facets for Highly Selective Tandem Electrocatalytic Carbon Dioxide Reduction. *Adv. Mater.* **2022**, *34* (19), 2110607. https://doi.org/10.1002/adma.202110607.
(25) Ma, S.; Sadakiyo, M.; Heima, M.; Luo, R.; Haasch, R. T.; Gold, J. I.; Yamauchi, M.; Kenis, P. J. A. Electroreduction of Carbon Dioxide to Hydrocarbons Using Bimetallic Cu–Pd Catalysts with Different Mixing Patterns. *J. Am. Chem. Soc.* **2017**, *139* (1), 47–50. https://doi.org/10.1021/jacs.6b10740.
(26) Lin, L.; Liu, T.; Xiao, J.; Li, H.; Wei, P.; Gao, D.; Nan, B.; Si, R.; Wang, G.; Bao, X. Enhancing CO_2 Electroreduction to Methane with a Cobalt Phthalocyanine and Zinc–Nitrogen–Carbon Tandem Catalyst. *Angew. Chem. Int. Ed.* **2020**, *59* (50), 22408–22413. https://doi.org/10.1002/anie.202009191.
(27) Akter, T.; Pan, H.; Barile, C. J. Tandem Electrocatalytic CO_2 Reduction inside a Membrane with Enhanced Selectivity for Ethylene. *J. Phys. Chem. C* **2022**, *126* (24), 10045–10052. https://doi.org/10.1021/acs.jpcc.2c01663.
(28) Ozden, A.; Wang, Y.; Li, F.; Luo, M.; Sisler, J.; Thevenon, A.; Rosas-Hernández, A.; Burdyny, T.; Lum, Y.; Yadegari, H.; Agapie, T.; Peters, J. C.; Sargent, E. H.; Sinton, D. Cascade CO_2 Electroreduction Enables Efficient Carbonate-Free Production of Ethylene. *Joule* **2021**, *5* (3), 706–719. https://doi.org/10.1016/j.joule.2021.01.007.
(29) Zhang, T.; Li, Z.; Zhang, J.; Wu, J. Enhance CO_2-to-C_{2+} Products Yield through Spatial Management of CO Transport in Cu/ZnO Tandem Electrodes. *J. Catal.* **2020**, *387*, 163–169. https://doi.org/10.1016/j.jcat.2020.05.002.
(30) She, X.; Zhang, T.; Li, Z.; Li, H.; Xu, H.; Wu, J. Tandem Electrodes for Carbon Dioxide Reduction into C_{2+} Products at Simultaneously High Production Efficiency and Rate. *Cell Rep. Phys. Sci.* **2020**, *1* (4), 100051. https://doi.org/10.1016/j.xcrp.2020.100051.
(31) Zhang, T.; Bui, J. C.; Li, Z.; Bell, A. T.; Weber, A. Z.; Wu, J. Highly Selective and Productive Reduction of Carbon Dioxide to Multicarbon Products via in Situ CO

Management Using Segmented Tandem Electrodes. *Nat. Catal.* **2022**, *5* (3), 202–211. https://doi.org/10.1038/s41929-022-00751-0.
(32) Romero Cuellar, N. S.; Scherer, C.; Kaçkar, B.; Eisenreich, W.; Huber, C.; Wiesner-Fleischer, K.; Fleischer, M.; Hinrichsen, O. Two-Step Electrochemical Reduction of CO_2 towards Multi-Carbon Products at High Current Densities. *J. CO2 Util.* **2020**, *36*, 263–275. https://doi.org/10.1016/j.jcou.2019.10.016.
(33) Feng, J.; Badreldin, A.; Li, Y. Electrochemical CO_2 Reduction to Multicarbon Fuels and Chemicals: Progress and Prospects of Tandem Electrolyzer Strategies. *Energy Fuels* **2025**, *39* (44), 21175–21225. https://doi.org/10.1021/acs.energyfuels.5c04464.
(34) Sassenburg, M.; Iglesias Van Montfort, H. P.; Kolobov, N.; Smith, W. A.; Burdyny, T. Bulk Layering Effects of Ag and Cu for Tandem CO_2 Electrolysis. *ChemSusChem* **2025**, *18* (8), e202401769. https://doi.org/10.1002/cssc.202401769.
(35) Chatterjee, T.; Boutin, E.; Robert, M. Manifesto for the Routine Use of NMR for the Liquid Product Analysis of Aqueous CO_2 Reduction: From Comprehensive Chemical Shift Data to Formaldehyde Quantification in Water. *Dalton Trans.* **2020**, *49* (14), 4257–4265. https://doi.org/10.1039/C9DT04749B.
(36) Prabhakar, R. R.; Lemerle, R.; Barecka, M.; Kim, M.; Seo, S.; Dayi, E. N.; Dei Tos, I.; Ager, J. W. TaO_x Electron Transport Layers for CO_2 Reduction Si Photocathodes. *J. Mater. Chem. A* **2023**, *11* (25), 13588–13599. https://doi.org/10.1039/D3TA01028G.
(37) Xu, Q.; Liu, S.; Longhin, F.; Kastlunger, G.; Chorkendorff, I.; Seger, B. Impact of Anodic Oxidation Reactions in the Performance Evaluation of High-Rate CO_2 /CO Electrolysis. *Adv. Mater.* **2024**, *36* (2), 2306741. https://doi.org/10.1002/adma.202306741.
(38) Agbo, P. Transparent Dual-Conductivity Membrane Composites as Current Distributors for Diffuse Electrocatalysts. *ACS Appl. Energy Mater.* **2020**, *3* (12), 12284–12290. https://doi.org/10.1021/acsaem.0c02339.
(39) Yahyaie, I.; Ardo, S.; Oliver, D. R.; Thomson, D. J.; Freund, M. S.; Lewis, N. S. Comparison between the Electrical Junction Properties of H-Terminated and Methyl-Terminated Individual Si Microwire/Polymer Assemblies for Photoelectrochemical Fuel Production. *Energy Environ. Sci.* **2012**, *5* (12), 9789. https://doi.org/10.1039/c2ee23115h.
(40) Abouremeleh, M. H.; Rivera, R. A.; Kistler, T. A.; Agbo, P. Durability Optimization of CO_2 Electrolyzers for Syngas Evolution. *J. Electrochem. Soc.* **2025**, *172* (7), 074513. https://doi.org/10.1149/1945-7111/adef84.
(41) Casebolt, R.; Levine, K.; Suntivich, J.; Hanrath, T. Pulse Check: Potential Opportunities in Pulsed Electrochemical CO_2 Reduction. *Joule* **2021**, *5* (8), 1987–2026. https://doi.org/10.1016/j.joule.2021.05.014.
(42) Watkins, N. B.; Wu, Y.; Nie, W.; Peters, J. C.; Agapie, T. *In Situ* Deposited Polyaromatic Layer Generates Robust Copper Catalyst for Selective Electrochemical CO_2 Reduction at Variable pH. *ACS Energy Lett.* **2023**, *8* (1), 189–195. https://doi.org/10.1021/acsenergylett.2c02002.
(43) Watkins, N. B.; Schiffer, Z. J.; Lai, Y.; Musgrave, C. B.; Atwater, H. A.; Goddard, W. A.; Agapie, T.; Peters, J. C.; Gregoire, J. M. Hydrodynamics Change Tafel Slopes in Electrochemical CO_2 Reduction on Copper. *ACS Energy Lett.* **2023**, *8* (5), 2185–2192. https://doi.org/10.1021/acsenergylett.3c00442.
(44) Jouny, M.; Hutchings, G. S.; Jiao, F. Carbon Monoxide Electroreduction as an Emerging Platform for Carbon Utilization. *Nat. Catal.* **2019**, *2* (12), 1062–1070. https://doi.org/10.1038/s41929-019-0388-2.

(45) Kistler, T. A.; Um, M. Y.; Cooper, J. K.; Sharp, I. D.; Agbo, P. Exploiting Heat Transfer to Achieve Efficient Photoelectrochemical CO_2 Reduction under Light Concentration. *Energy Environ. Sci.* **2022**, *15* (5), 2061–2070. https://doi.org/10.1039/D1EE03957A.
(46) Qu, J.; Cao, X.; Gao, L.; Li, J.; Li, L.; Xie, Y.; Zhao, Y.; Zhang, J.; Wu, M.; Liu, H. Electrochemical Carbon Dioxide Reduction to Ethylene: From Mechanistic Understanding to Catalyst Surface Engineering. *Nano-Micro Lett.* **2023**, *15* (1), 178. https://doi.org/10.1007/s40820-023-01146-x.
(47) Jiang, R.; Parameshwaran, V. S.; Boltersdorf, J.; Baker, D. R. Copper-Nanowires Incorporated with Silver-Nanoparticles for Catalytic CO_2 Reduction in Alkaline Zero Gap Electrolyzer. *ACS Appl. Energy Mater.* **2023**, *6* (20), 10475–10486. https://doi.org/10.1021/acsaem.3c01605.
(48) Zhelyabovskiy, M.; Jung, H.; Diaconescu, P. L.; Peters, J. C.; Agapie, T. Plastic from CO_2, Water, and Electricity: Tandem Electrochemical CO_2 Reduction and Thermochemical Ethylene-CO Copolymerization. *Angew. Chem. Int. Ed.* **2025**, *64* (24), e202503003. https://doi.org/10.1002/anie.202503003.
(49) Zhang, H.; Raciti, D.; Hall, A. S. Disordered Interfacial H_2O Promotes Electrochemical C–C Coupling. *Nat. Chem.* **2025**, *17* (8), 1161–1168. https://doi.org/10.1038/s41557-025-01859-z.